JACS
JOURNAL OF THE AMERICAN CHEMICAL SOCIETY

Communication

pubs.acs.org/JACS

Five-Fold Twinned Pd_2NiAg Nanocrystals with Increased Surface Ni Site Availability to Improve Oxygen Reduction Activity

Suli Liu,[†] Qinghua Zhang,[‡] Yafei Li,[†] Min Han,[†] Lin Gu,*[,§,∥] Cewen Nan,[‡] Jianchun Bao,[†] and Zhihui Dai*[,†]

[†]Jiangsu Collaborative Innovation Center of Biomedical Functional Materials and Jiangsu Key Laboratory of Biofunctional Materials, School of Chemistry and Materials Science, Nanjing Normal University, Nanjing 210023, P. R. China

[‡]Department of Materials Science and Engineering, State Key Lab of New Ceramics and Fine Processing, Tsinghua University, Beijing 100084, P. R. China

[§]Beijing National Laboratory for Condensed Matter Physics, Institute of Physics, Chinese Academy of Sciences, Beijing 100190, P. R. China

[∥]Collaborative Innovation Center of Quantum Matter, Beijing 100190, P. R. China

Supporting Information

ABSTRACT: The synthesis of highly active oxygen reduction reaction (ORR) catalysts with good durability and low cost is highly desirable but still remains a significant challenge. In this work, we present the synthesis of five-fold twinned Pd_2NiAg nanocrystals (NCs) with a Ni-terminal surface which exhibit excellent electrocatalytic performance for ORR in alkaline media, even better than the performance of the commercial Pt/C catalyst. Using high-angle annular-dark-field imaging together with density functional theory calculations, it is found that the surfaces of the five-fold twinned Pd_2NiAg NCs exhibit an unusual valence electron density. The maximum catalytic activity originates from the increased availability of surface Ni sites in five-fold twinned Pd_2NiAg NCs and the features of twinned structural defects. This study provides an explanation of the enhanced ORR from the special structure of this novel material, which opens up new avenues for the design of novel classes of electrocatalysts for fuel cells and metal−air batteries.

Electrochemical energy conversion devices ranging from fuel cells to metal−air batteries demand effective electrocatalysts for oxygen reduction reaction (ORR).[1−5] Studies of bimetallic Pt-M alloy nanocrystals (NCs) in which M is a transition metal (M = Fe, Co, and Ni) have demonstrated intrinsic ORR activities that are several times higher than those of pure Pt.[6−8] This catalytic enhancement is ascribed to optimization of the absorption energy between oxygen and Pt via strain and ligand effects.[8−11] However, the practical large-scale commercialization of fuel cells remains a significant challenge partially due to the high price, limited supply, and sluggish ORR process of Pt-based catalysts during operation.[6,12−14] Therefore, the design of non-Pt electrocatalysts with improved catalytic activity and durability is highly desirable. Furthermore, it is important to understand the correlation of non-Pt electrocatalyst architectures with the desired catalytic properties of high activity and durability.

The typical structure of five-fold twinned NCs is a pentagonal prism with {100} facets capped by two pentagonal pyramids with {111} facets. They are frequently observed in metal and binary alloy NCs due to their crystal structure features (e.g., face-centered cubic metals).[15,16] However, due to the notably high stacking fault energy and lattice mismatch of ternary alloy NCs, twinned ternary alloy NCs have rarely been obtained. Recent research on twinned NCs has led to certain exciting advances in understanding the catalytic nature of materials,[17,18] thus allowing more rational tuning of catalytic properties (e.g., accelerating the sluggish ORR) via control of twin defect sites. More importantly, the composition of the topmost surface atomic layers in the five-fold twinned NCs might alter the kinetics of ORR. Here, considering the minimally different atomic radii of Pd and Ag, while Ni has a much smaller radius than those of Pd and Ag, we present the synthesis of five-fold twinned Pd_2NiAg NCs with a Ni-terminal surface, which exhibits excellent electrocatalytic performance for ORR in alkaline media, even better than the performance of the commercial Pt/C catalyst.

Five-fold twinned Pd_2NiAg NCs were synthesized via the solid−liquid phase chemical route [see Supporting Information (SI)]. By adjusting the molar ratio of the introduced Pd/Ni/Ag solid precursors, five-fold twinned Pd_2NiAg NCs were easily obtained. Transmission electron microscopy (TEM) images show that the size of the as-synthesized five-fold twinned Pd_2NiAg NCs is ∼15 nm (Figure S1a). A five-fold twinned particle outlined by five yellow dotted lines is shown in Figure 1a. Figure 1b, which displays the Fast Fourier Transform (FFT) image of Figure 1a, clearly illustrates the characteristic of 10-fold symmetry, as indicated by ten yellow circles. The structural model of this five-fold twinned crystal is presented in Figure 1c; a side view of the five-fold twinned crystal is also provided. As shown in Figure 1d, we observe two regions in the image: the region on the left is the ⟨114⟩ orientation, and the region on the right is the ⟨110⟩ orientation. The respective structure models along these two directions overlap on the high-angle annular-dark-field (HAADF) image. The FFT image in Figure 1e also demonstrates the superposition of the ⟨114⟩ and ⟨110⟩ directions, and the diffraction spots of the ⟨114⟩ orientation

Received: December 19, 2014
Published: January 28, 2015

DOI: 10.1021/ja5129154
J. Am. Chem. Soc. 2015, 137, 2820−2823

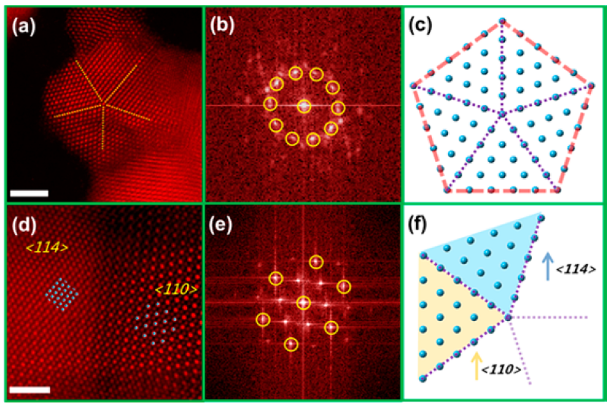

Figure 1. (a) HAADF image of Pd_2NiAg NCs with five-fold twinning, as outlined by five yellow dotted lines. The white scale bar in (a) is 2 nm. (b) Corresponding FFT image of (a) in which a set of ten-fold symmetric positions is indicated by yellow circles. (c) Structural model for five-fold twinning in agreement with the atomic projections in (a); for clarification, only one type of colored sphere is used. (d) HAADF image viewed along the ⟨114⟩ and ⟨110⟩ directions perpendicular to the five-fold twinned axis; structural models of Pd_2NiAg along the ⟨114⟩ and ⟨110⟩ directions overlap on the image. The corresponding FFT image in (e) also demonstrates the overlap between the ⟨110⟩ and ⟨114⟩ directions; yellow circles indicate the diffraction spots belonging to the atomic projection along the ⟨114⟩ direction. The white scale bar in (d) is 1 nm. (f) Structural schematics for the superposition of the ⟨110⟩ and ⟨114⟩ directions, indicating that they represent two branches of a five-fold twinned crystal.

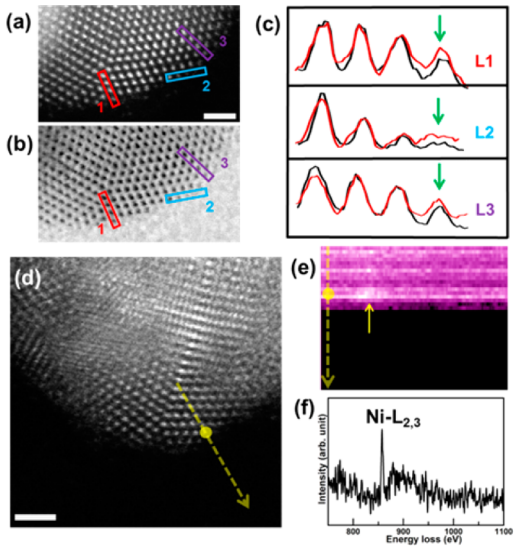

Figure 2. (a) HAADF and (b) ABF images of a five-fold twinned crystal, respectively; positions of three line profiles from the inside to the surface of Pd_2NiAg NCs are indicated by different colors, and the scale bar in (a) is 1 nm. (c) Corresponding line profiles of image contrast in HAADF and ABF images, indicated by black and red lines, respectively. The contrast of the ABF image is inversed for comparison. (d) HAADF image of a five-fold twinned crystal in which the position for EELS line scanning is indicated with a yellow dotted arrow; the scale bar in (d) is 1 nm. (e) A spectrum line-scan image with an energy range from 850 to 880 eV; the dotted yellow arrow on the left indicates the line-scan direction, and the small yellow arrow labels the relatively strong Ni-L2,3 signal on the surface. (f) Ni-L2,3 edge extracted at the surface region indicated by the yellow dot on the yellow arrow in (d).

are indicated with yellow circles. The schematic diagram of the orientation relationship between the ⟨114⟩ and ⟨110⟩ is shown in Figure 1f. The angle between the ⟨114⟩ and ⟨110⟩ in the cubic lattice is ~70.5°, which is close to the 72° of a five-fold twin. Thus, the HAADF image in Figure 1d suggests that the structures represent two branches of a five-fold twinned crystal.

Typical face-centered cubic structures are indicated by the X-ray diffraction (XRD) patterns in Figure S1b. According to Vegard's law, the atom percentages of Pd, Ni, and Ag in this sample are calculated as approximately 50%, 25%, and 25%, respectively, which are consistent with the data obtained from Induction Coupled Plasma Quantometer (ICP) measurements (49.4% for Pd, 25.3% for Ni, and 25.3% for Ag).

The five-fold twinned Pd_2NiAg NCs are also characterized using aberration-corrected scanning transmission electron microscopy (STEM) and STEM-electron energy-loss spectroscopy (STEM-EELS). We performed HAADF and angular bright-field (ABF) imaging simultaneously on the five-fold twinned Pd_2NiAg NCs, as shown in Figure 2a and b, respectively. Three line profiles of image intensity are measured on both HAADF and ABF images. A remarkable enhancement of contrast at the outmost layer of the twinned crystal in ABF image can be clearly identified, as indicated by green arrows shown in Figure 2c. Because the contrast of the HAADF image is proportional to $\sim Z^{1.7}$ of the element, whereas that of ABF images is $\sim Z^{1/3}$, this contrast enhancement should be attributed to the enrichment of Ni on the surface because Ni has the smallest Z number compared with Pd and Ag. To confirm this point, we perform elemental mapping and STEM-EELS line scans on the as-prepared five-fold twinned Pd_2NiAg NCs (Figure S1c and Figure 2d). The yellow dotted arrow in Figure 2d indicates the scanning positions from the inside to the surface of this five-fold twin crystal. The Ni signal becomes stronger near the surface, as indicated by the small yellow arrow in Figure 2e. Figure 2f displays the obvious Ni-L2,3 peak on the surface region. Based on the experimental observations from imaging and spectroscopy, we conclude that a Ni-rich layer exists on the topmost surface of the five-fold twinned Pd_2NiAg NCs.

The electrocatalytic ORR performances of five-fold twinned Pd_2NiAg NCs are investigated using rotating disk voltammetry (RDV) in O_2-saturated 0.1 M KOH solutions. Figure 3a shows the corresponding ORR polarization curve at a rotation rate of 1600 rpm. For comparison, under the same experimental conditions, the ORR polarization curves for spherical Pd_2NiAg NCs, five-fold twinned Pd_2Ag NCs and commercial Pt/C catalysts are also given. The characterizations of spherical Pd_2NiAg NCs and five-fold twinned Pd_2Ag NCs have been shown in Figures S2 and S3, respectively. The polarization curves display a diffusion-limiting current region from −0.6 V to −0.2 V and a mixed kinetic-diffusion control region between approximately −0.2 and 0 V.[10,19] The onset reduction potential of five-fold twinned Pd_2NiAg NCs is approximately −0.05 V (vs Ag/AgCl), which is more positive than that of spherical Pd_2NiAg NCs (−0.10 V), five-fold twinned Pd_2Ag NCs (−0.15 V), and commercial Pt/C (−0.08 V) catalysts (Figure 3a). The magnified potential region from −0.2 to 0 V is shown in Figure S4. Additionally, the half-wave potential ($E_{1/2}$) of five-fold twinned Pd_2NiAg NCs (−0.131 V) is higher than that of spherical Pd_2NiAg NCs (−0.136 V), five-fold twinned Pd_2Ag NCs (−0.220 V), and commercial Pt/C catalysts (−0.137 V). These results reveal that the five-fold twinned Pd_2NiAg NCs catalyst possesses the highest catalytic performance compared with those of the other two control catalysts and the commercial Pt/C catalyst. To obtain further insight into the catalytic behaviors of these materials, electrocatalytic dynamic experiments are further

DOI: 10.1021/ja5129154
J. Am. Chem. Soc. 2015, 137, 2820−2823

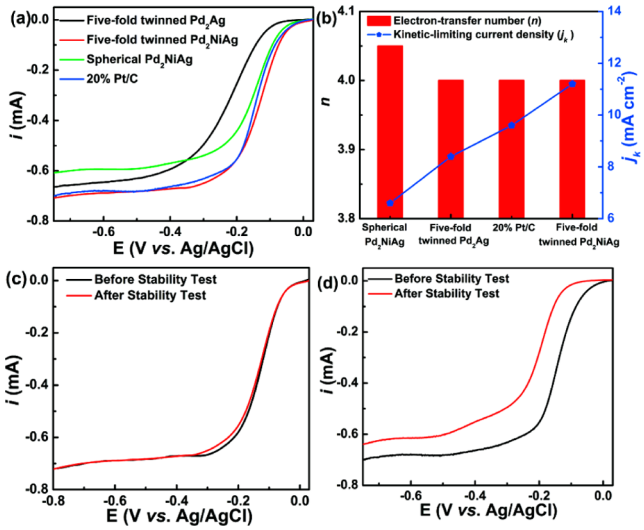

Figure 3. (a) Polarization curves for ORR in O_2-saturated 0.1 M KOH solution; scan rate: 5 mV/s and rotation rate: 1600 rpm. (b) Electron transfer number and kinetic-limiting current density of the five-fold twinned Pd_2NiAg NCs, spherical Pd_2NiAg NCs, five-fold twinned Pd_2Ag NCs, and commercial Pt/C catalysts at −0.50 V (vs Ag/AgCl). ORR polarization curves of the five-fold twinned Pd_2NiAg NCs (c) and commercial Pt/C (d) catalyst before and after 5000 potential sweeps between −0.8 and 0.1 V, respectively.

performed by measuring ORR polarization plots under different rotation rates, from which the Koutecky−Levich (K−L) plots at different potentials can be obtained. Based on the slopes of the K−L plots, the electron transfer number (n) involved in the ORR process for these catalysts is calculated as ∼4 at −0.50 V (vs Ag/AgCl) (Figure S5),[20] indicating that the ORR mechanism on those catalysts follows the direct "4e−" pathway ($O_2 + 2H_2O + 4e^- = 4OH^-$).[21] Although ORR mechanisms of these catalysts are identical, their kinetic-limiting current density (j_k) values (Figure 3b) are quite different. In contrast to five-fold twinned Pd_2Ag NCs, spherical Pd_2NiAg NCs, and commercial Pt/C catalyst, the five-fold twinned Pd_2NiAg NCs exhibit a much higher kinetic-limiting current density, indicating that the Ni-terminal surface in five-fold twinned Pd_2NiAg NCs is able to dramatically enhance the electrocatalytic ORR performance. Previous theoretical and experimental works[6−8,22−25] demonstrated that Pt−M alloy NCs (M = Fe, Co, and Ni) down-shift the d-band center of Pt, which weakened the adsorption of oxygenated intermediates and released additional active sites on Pt and was beneficial to improve ORR performance. In our work, a Ni-terminal surface with an optimal valence electron density (via changing the d-band center and the band spacing) plays a significant role in ORR. The Ni terminal surface solves the O_2 adsorption and desorption, two completely diverse valence electron demands, reaching a new equilibrium state.

Except for the catalytic activity, the long-term stability or durability is another important parameter that determines the practical application of a specific ORR electrocatalyst. Durability tests of five-fold twinned Pd_2NiAg NCs (Figure 3c) and commercial Pt/C (Figure 3d) catalysts are further performed by cycling the potential between −0.8 and 0.1 V (vs Ag/AgCl) in O_2-saturated 0.1 M KOH with a scan rate of 100 mV/s.[10] After 5000 continuous cycles, the five-fold twinned Pd_2NiAg NCs catalyst shows a slight variation from that of the commercial Pt/C catalyst, implying that the five-fold twinned Pd_2NiAg NCs also possess excellent cycling stability or durability. Using TEM to analyze the catalyst after the durability test, we find that the morphology and composition of this catalyst are almost unchanged (Figure S6), which might be the origin of the observed excellent stability for this catalyst. This work highlights the significant potential of five-fold twinned Pd_2NiAg NCs as a highly efficient electrocatalyst for ORR (Table S1)[10,19,25−30] and its potential for use as a substitute Pt/C catalyst for application in alkaline fuel cells.

Generally, Pt skin (preparing core/shell nanostructures with Pt atoms only located in a thin shell) is able to catalyze ORR effectively.[8−11] Nevertheless, in this work, the increased surface Ni site availability in five-fold twinned Pd_2NiAg NCs governs the maximum catalytic activity for ORR for which a balance can be achieved only with an optimal valence electron density level. To prove this point of view, we use density functional theory (DFT) computations to analyze the oxygen adsorption energy (E_O), a commonly used descriptor for ORR activity, on different types of NCs surfaces.[6,10,31−33] We use $Pd_{37}Ag_{18}$ and $Pd_{27}Ni_{14}Ag_{14}$ clusters to represent five-fold twinned Pd_2Ag NCs and five-fold twinned Pd_2NiAg NCs, respectively.[34,35] Because oxygen overbinds to five-fold twinned Pd_2Ag NCs and Ni surfaces (ΔE_O is negative), the goal is to design five-fold twinned Pd_2NiAg NCs with less negative ΔE_O values to achieve higher ORR activities.[31] First, we focus on the dependence of ΔE_O on the surface valence electron density of five-fold twinned Pd_2NiAg NCs. Figure 4a depicts ΔE_O as a function of the surface valence

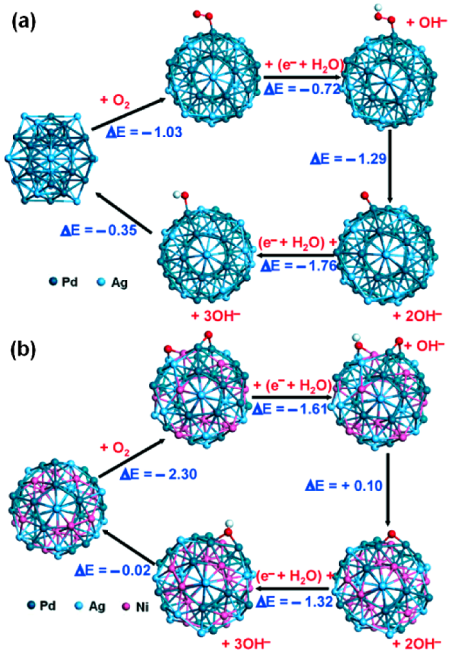

Figure 4. Attachment of an oxygen molecule on the five-fold twinned Pd_2Ag NCs (a) and five-fold twinned Pd_2NiAg NCs (b), respectively.

electron density (Figure S7) of the five-fold twinned Pd_2Ag NCs (ΔE_O = −0.35 eV). The Pd and Ag atoms at the first layer are displaced by Ni, and the topmost surface becomes layered with Ni, where the ΔE_O is −0.02 eV (Figure 4b), which is much smaller (in absolute value) than the value for five-fold twinned Pd_2Ag NCs. These results demonstrate that the Ni skin in a five-fold twinned Pd_2Ag NCs substrate would be a perfect architecture, allowing the ΔE_O to decrease relative to that of the five-fold twinned Pd_2Ag NCs. The data strongly support the existence of a surface valence electron effect, whereby a suitable

DOI: 10.1021/ja5129154
J. Am. Chem. Soc. 2015, 137, 2820−2823

geometric arrangement of five-fold twinned Pd_2NiAg NCs surface atoms catalyzes ORR.

In summary, five-fold twinned Pd_2NiAg NCs with a Ni-terminal surface are prepared by the solid−liquid phase chemical route and shown to exhibit higher ORR performance compared with those of the commercial Pt/C. Based on these results, we provide an advanced viewpoint that could be used to understand the variations in ORR performance caused by the surface valence electron density, structural defects, and the feasibility of tailoring the surface Ni site availability of the five-fold twinned Pd_2NiAg NCs. In the future, the findings of this work could be used to predict the optimal structure for maximum ORR activity and to guide synthetic control of the defect structure of the twinned ternary NCs via an understanding of the correlation between the surface defects of five-fold twinned Pd_2NiAg NCs and the resulting ORR performance.

■ ASSOCIATED CONTENT

Supporting Information

Details of experiments, structural characterizations, and DFT calculations. This material is available free of charge via the Internet at http://pubs.acs.org.

■ AUTHOR INFORMATION

Corresponding Authors

*daizhihuii@njnu.edu.cn

*l.gu@iphy.ac.cn

Notes

The authors declare no competing financial interest.

■ ACKNOWLEDGMENTS

We thank the financial support from the NSFC (Nos. 21175069, 21171096, 21475062, 51332001, 21271105, and 21403115), Strategic Priority Research Program of the Chinese Academy of Sciences (Grant No. XDB07030200), and PAPD.

■ REFERENCES

(1) Steele, B. C. H.; Heinzel, A. *Nature* **2001**, *414*, 345−352.

(2) Wu, J.; Yang, H. *Acc. Chem. Res.* **2013**, *46*, 1848−1857.

(3) Kim, T. W.; Choi, K. S. *Science* **2014**, *343*, 990−994.

(4) Zhang, M.; de Respinis, M.; Frei, H. *Nat. Chem.* **2014**, *6*, 362−367.

(5) Liu, M. M.; Zhang, R. Z.; Chen, W. *Chem. Rev.* **2014**, *114*, 5117−5160.

(6) Stamenkovic, V. R.; Fowler, B.; Mun, B. S.; Wang, G. F.; Ross, P. N.; Lucas, C. A.; Marković, N. M. *Science* **2007**, *315*, 493−497.

(7) Subbaraman, R.; Tripkovic, D.; Chang, K. C.; Strmcnik, D.; Paulikas, A. P.; Hirunsit, P.; Chan, M.; Greeley, J.; Stamenkovic, V.; Markovic, N. M. *Nat. Mater.* **2012**, *11*, 550−557.

(8) Zhang, S.; Hao, Y. Z.; Su, D.; Doan-Nguyen, V. V. T.; Wu, Y. T.; Li, J.; Sun, S. H.; Murray, C. B. *J. Am. Chem. Soc.* **2014**, *136*, 15921−15924.

(9) Mavrikakis, M.; Hammer, B.; Nørskov, J. K. *Phys. Rev. Lett.* **1998**, *81*, 2819.

(10) Guo, S. J.; Zhang, X.; Zhu, W. L.; He, K.; Su, D.; Mendoza-Garcia, A.; Ho, S. F.; Lu, G.; Sun, S. H. *J. Am. Chem. Soc.* **2014**, *136*, 15026−15033.

(11) Wang, X. M.; Orikasa, Y.; Takesue, Y.; Inoue, H.; Nakamura, M.; Minato, T.; Hoshi, N.; Uchimoto, Y. *J. Am. Chem. Soc.* **2013**, *135*, 5938−5941.

(12) Gong, K. P.; Du, F.; Xia, Z. H.; Durstock, M.; Dai, L. M. *Science* **2009**, *323*, 760−764.

(13) Waki, K.; Wong, R. A.; Oktaviano, H. S.; Fujio, T.; Nagai, T.; Kimoto, K.; Yamada, K. *Energy Environ. Sci.* **2014**, *7*, 1950−1958.

(14) Liu, M. M.; Zhang, R. Z.; Chen, W. *Chem. Rev.* **2014**, *114*, 5117−5160.

(15) Tian, M.; Wang, J.; Kurta, J.; Mallouk, T. E.; Chan, M. H. W. *Nano Lett.* **2003**, *3*, 91−923.

(16) Abe, E. *Chem. Soc. Rev.* **2012**, *41*, 6787−6798.

(17) Zhou, Z. Y.; Tian, N.; Li, J. T.; Broadwell, I.; Sun, S. G. *Chem. Soc. Rev.* **2011**, *40*, 4167−4185.

(18) Long, R.; Zhou, S.; Wiley, B. J.; Xiong, Y. J. *Chem. Soc. Rev.* **2014**, *43*, 6288−6310.

(19) Yin, H. J.; Tang, H. J.; Wang, D.; Gao, Y.; Tang, Z. Y. *ACS Nano* **2012**, *6*, 8288−8297.

(20) Wang, S.; Zhang, L.; Xia, Z.; Roy, A.; Chang, D. W.; Baek, J.-B.; Dai, L. *Angew. Chem., Int. Ed.* **2012**, *51*, 4209−4212.

(21) Byers, J. C.; Güell, A. G.; Unwin, P. R. *J. Am. Chem. Soc.* **2014**, *136*, 11252−11255.

(22) Gan, L.; Heggen, M.; Rudi, S.; Strasser, P. *Nano Lett.* **2012**, *12*, 5423−5430.

(23) Choi, C. H.; Park, S. H.; Woo, S. I. *Appl. Catal., B* **2012**, *119*, 123−131.

(24) Han, B. H.; Carlton, C. E.; Kongkanand, A.; Kukreja, R. S.; Theobald, B. R.; Gan, L.; O'Malley, R.; Strasser, P.; Wagner, F. T.; Shao-Horn, Y. *Energy Environ. Sci.* **2015**, *8*, 258−266.

(25) Peng, H. L.; Liu, F. F.; Liu, X. J.; Liao, S. J.; You, C. H.; Tian, X. L.; Nan, H. X.; Luo, F.; Song, H. Y.; Fu, Z. Y.; Huang, P. Y. *ACS Catal.* **2014**, *4*, 3797−3805.

(26) Liang, J.; Jiao, Y.; Jaroniec, M.; Qiao, S. Z. *Angew. Chem.* **2012**, *124*, 11664−11668.

(27) Sohn, G. J.; Choi, H. J.; Jeon, I. Y.; Chang, D. W.; Dai, L. M.; Baek, J. B. *ACS Nano* **2012**, *6*, 6345−6355.

(28) Wu, Z. S.; Yang, S. B.; Sun, Y.; Parvez, K.; Feng, X. L.; Müllen, K. *J. Am. Chem. Soc.* **2012**, *134*, 9082−9085.

(29) Li, Y.; Zhao, Y.; Cheng, H. H.; Hu, Y.; Shi, G. Q.; Dai, L. M.; Qu, L. T. *J. Am. Chem. Soc.* **2012**, *134*, 15−18.

(30) Fadil, N. A.; Saravanan, G.; Ramesh, G. V.; Matsumoto, F.; Yoshikawa, H.; Ueda, S.; Tanabe, T.; Hara, T.; Ishihara, S.; Murakami, H.; Arigagh, K.; Abe, H. *Chem. Commun.* **2014**, *50*, 6451−6453.

(31) Suo, Y. E.; Zhuang, L.; Lu, J. T. *Angew. Chem., Int. Ed.* **2007**, *46*, 2862−2864.

(32) Hwang, S. J.; Kim, S. K.; Lee, J. G.; Lee, S. C.; Jang, J. H.; Kim, P.; Lim, T. H.; Sung, Y. E.; Jong Yoo, S. J. *J. Am. Chem. Soc.* **2012**, *134*, 19508−19511.

(33) Slanac, D. A.; Hardin, W. G.; Johnston, K. P.; Stevenson, K. J. *J. Am. Chem. Soc.* **2012**, *134*, 9812−9819.

(34) Gao, Y.; Shao, N.; Pei, Y.; Zeng, X. C. *Nano Lett.* **2010**, *10*, 1055−1062.

(35) Huang, X.; Qi, X. Y.; Huang, Y. Z.; Li, S. Z.; Xue, C.; Gan, C. L.; Boey, F.; Zhang, H. *ACS Nano* **2010**, *4*, 6196−6202.

DOI: 10.1021/ja5129154
J. Am. Chem. Soc. 2015, 137, 2820−2823